

MODELING OF CRITICAL WEATHER FLIGHT PERFORMANCE OF MULTICOPTER UAVS FOR RESILIENT CONTROLLER DESIGN.

Arno Fallast[1,2] & Samuel Lesak[1]

[1]FH JOANNEUM, Institute of Aviation, Graz
[2]Graz University of Technology, Institute of Machine Learning and Neural Computation

Abstract

Aircraft icing is a critical safety hazard for urban air mobility (UAM) vehicles and unmanned aerial vehicles (UAVs), particularly for multicopter platforms operating at low altitude in adverse meteorological conditions. Operational and regulatory limitations related to icing can significantly reduce UAV availability during cold-weather seasons, directly affecting emergency response, infrastructure inspection, and other time-critical missions. Despite advances in numerical simulation and component-level testing, experimentally supported models that connect propeller icing, propulsion degradation, and controller-oriented UAV simulation remain scarce for small multicopters. This paper presents an experimentally driven and control-oriented investigation of multicopter UAV operation under icing-induced propulsion degradation. Experiments are conducted in a large-scale calibrated climatic and icing wind tunnel using a fixed test-stand setup of a quadrotor UAV mock-up in the sub-$10\,\mathrm{kg}$ maximum take-off mass class at a representative forward-flight condition of $10\,\mathrm{m\,s^{-1}}$. The experimental campaign is combined with prior motor-propeller icing data to obtain a data-driven degradation representation for the present propulsion configuration. The resulting model is embedded in a six-degree-of-freedom UAV simulation and used to evaluate actuator usage under degraded propulsion performance. The results show that icing-induced propeller degradation leads to a pronounced increase in required motor command and electrical power demand. For a maximum-payload UAV configuration, simulations with pre-accreted ice indicate operation close to the available actuator command limit when using a fixed-gain baseline controller. An optimized degradation-aware controller, combining adapted feedback gains with modified reference velocities, reduces the required actuator usage during the considered evasive manoeuvre. The study therefore demonstrates a pathway from experimental icing observations to controller-oriented degradation modelling and resilient control adaptation for multicopter UAVs.

Novelty and Contribution

The primary contributions of this work are: (i) a full-UAV wind-tunnel test-stand methodology for repeatable investigation of multicopter propulsion degradation under controlled icing conditions; (ii) a prior-based, data-driven adaptation of an icing-induced motor-propeller degradation model to the present propulsion configuration; and (iii) a controller-oriented simulation study showing how degradation-aware control adaptation can reduce actuator usage during an evasive manoeuvre after ice accretion. Together, these contributions address a key gap between component-level icing tests, full-UAV experimental observations, and controller-oriented evidence for adverse-weather UAV operation.

Keywords: UAV icing, free-flight wind-tunnel testing, outdoor flight testing, adverse weather, health monitoring

1. Introduction

Adverse weather conditions remain a major limitation for unmanned aerial vehicles (UAVs), manned aircraft, and emerging urban air mobility (UAM) concepts. In particular, icing conditions can severely restrict the operational availability of small UAVs, since many commercial systems are not certified or technically equipped for flight in freezing precipitation, low temperatures, or icing clouds. Restrictions

imposed by manufacturers, operational procedures, or regulatory constraints can therefore substantially reduce the number of weather-permissible flight windows. Gao et al. report that, for UAVs without specific adverse-weather protection measures, the availability for legal flight can be reduced to below $30\,\%$ during the cold season in many regions of the world, and remains below $85\,\%$ in the cold season even for drones with enhanced weather resistance in regions beyond 45°N or -45°S [1]. This motivates the development of methods that enable safer UAV operation under adverse weather conditions, including ice-detection, degradation modelling, and controller adaptation.

The operational relevance of icing for future UAM services is further underlined by the Global Icing Report by Unisphere, which analysed icing potential for 30 UAM-relevant cities worldwide [2]. The report shows strong seasonal, regional, and altitude-dependent differences in icing occurrence. For many European locations, the highest icing potential is reported from December to February, whereas icing conditions are rare from May to September. Similar seasonal trends are reported for North America, where several locations show relevant icing potential from November to March. In Asia, the report identifies strong regional differences, with Astana and Sapporo showing particularly high icing exposure. The report also highlights that icing potential may increase sharply with altitude, even when near-surface conditions appear less critical. Although the study uses a conservative weather-based criterion based on temperature and relative humidity, and does not explicitly include droplet-size or cloud microphysics information, it demonstrates that icing can represent a substantial operational constraint for aircraft without ice-protection systems.

Aircraft icing is commonly investigated under defined atmospheric icing envelopes, most prominently the conventional icing conditions described in Appendix C to CS-25 and the supercooled-large-droplet conditions described separately in Appendix O [3]. Icing wind-tunnel experiments provide controlled and repeatable conditions for studying the underlying accretion processes and their effect on aircraft components. While much of the classical icing literature focuses on fixed-wing aircraft, lifting surfaces, and ice-protection systems, multicopter UAVs introduce an additional challenge: their lift and control authority are generated directly by rotating propellers whose aerodynamic performance can change rapidly under ice accretion. In the present work, Appendix-C-type icing conditions are used as a recognized atmospheric icing reference, but the study is not intended as a certification campaign.

For vertical takeoff and landing (VTOL) capable multicopter UAVs, propulsion is typically provided by commercial off-the-shelf brushless direct current (BLDC) motors in combination with lightweight propellers and electronic speed controllers. BLDC motors are widely used in automotive, industrial, robotic, and autonomous systems, and a large body of literature addresses classical BLDC faults. These faults are commonly classified into electrical faults, such as sensor, driver, or stator-winding faults; magnetic faults, such as demagnetization; and mechanical faults, such as eccentricities, broken rotor bars, or bearing failures [4, 5]. In multicopter icing, however, the dominant degradation mechanism considered here is not necessarily a fault of the electric motor itself, but an icing-induced change of the coupled motor–propeller–airframe behaviour.

Studies report similar degradation mechanisms. Orchard developed dedicated icing-test facilities for RPAS rotors and full RPAS operation in icing conditions, showing that ice accretion on propellers can lead to rapid thrust degradation, increased torque demand, and substantially higher electrical power consumption [6, 7]. In rotor-level tests, the increased power demand was observed while attempting to maintain prescribed thrust under Appendix-C, freezing-drizzle, and freezing-rain conditions [8]. In full-RPAS hover tests, increased motor power and loss of sustained hover capability were reported after exposure to calibrated icing sprays. These findings support the interpretation of multicopter icing as an actuator-effectiveness degradation rather than merely as an external aerodynamic disturbance. The present work provides direct experimental evidence of the same behaviour from the full-scale multicopter mock-up icing campaign conducted as part of this research. One of the key results of the campaign, illustrated by the representative dataset is the clear increase in propulsion-system demand

during icing exposure (see Figure 1). During the cloud-on interval, the commanded motor effort, motor current, and motor speed increase while the measured vertical force is initially maintained. This demonstrates that the propulsion system actively compensates for the degraded propeller state by drawing additional electrical power in order to preserve thrust. As the measurements originate from the authors' own full mock-up test campaign, they provide an important experimental foundation for the degradation modelling approach adopted in this paper. The observed reduction in propulsion margin directly motivates the use of degradation-aware simulation models and gain-scheduled control laws.

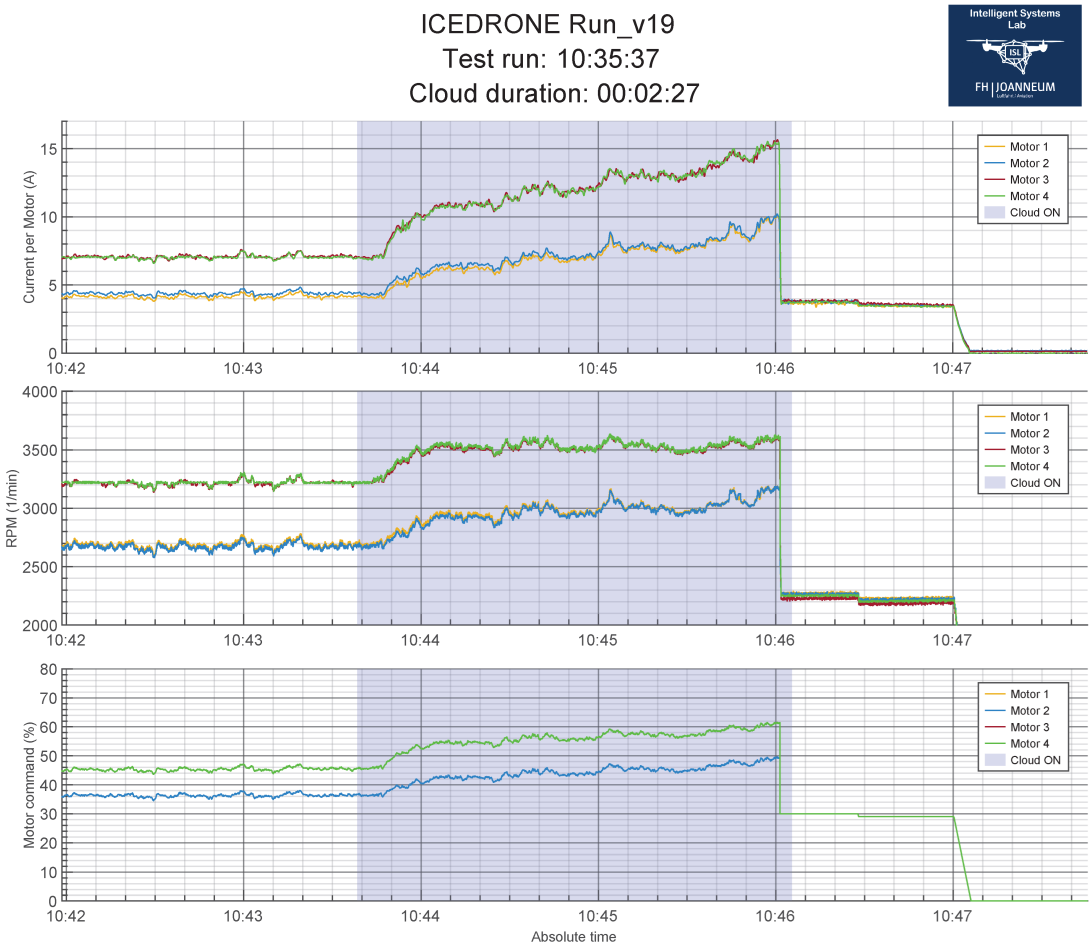


Figure 1 – Representative icing test run showing motor current, motor command, and motor speed during the icing-cloud interval. The shaded region indicates the active icing cloud. During this interval, the motor currents, commands, and rotational speeds increase markedly, indicating a pronounced increase in electrical power demand as the propulsion system compensates for icing-induced degradation. The effect is stronger on the faster rotating rear propellers, as they accumulate more ice.

Multicopter platforms are particularly sensitive to such degradation because their flight performance and control authority depend directly on the aerodynamic and dynamic characteristics of the rotor–motor–propeller system [9, 10]. Ice accretion on the propeller blades changes the effective blade geometry, reduces propulsive efficiency, increases torque demand, and may introduce additional vibration and imbalance. As a consequence, the same commanded motor input no longer produces the same thrust and moment response as under clean conditions. From the perspective of the flight controller, icing therefore acts as a time-varying actuator degradation and changes the mapping between motor commands and the generalized forces and moments acting on the vehicle [11].
For conventional multicopter flight controllers, these changes are problematic because the controller design is typically based on nominal actuator effectiveness and clean-airframe dynamics . Under

icing conditions, the available thrust margin, the motor time constants, the electrical power demand, and the achievable control moments may change substantially [6]. This can lead to degraded tracking performance, reduced stability margins, or, in severe cases, controller failure.
The present work builds on previous experimental and data-driven research on icing-induced multicopter powertrain degradation. In earlier work, a DMDc-based degradation model was identified from icing wind-tunnel experiments on a motor–propeller configuration and combined with software-based ice detection using propulsion-system telemetry [11]. In the present study, this prior knowledge is combined with newly acquired full-UAV wind-tunnel test-stand data and additional information from different test configurations and fidelity levels. The objective is to obtain a simulation-oriented degradation representation that incorporates the relevant propulsion effects and can be used to analyse the impact of icing on the UAV-level dynamic response.

The objective of this paper is to establish a model-based path towards resilient controller design. The current study combines information from previous motor–propeller icing experiments, full-UAV wind-tunnel test-stand measurements, and data-driven degradation modelling in order to derive a degradation-aware simulation model for performance analysis and gain-scheduled control. In this control concept, the feedback gains are adapted as a function of the current degradation state. Since scheduled gain values require at least an approximate indication of the current degradation level, an ice-mass-based scheduling coordinate is used as a virtual degradation indicator. This links the observed propulsion-system telemetry and the degradation model to the controller-design workflow. Lastly the objective is to prevent actuator saturation, which is a critical failure mode for LQR-based controllers, by incorporating a saturation-aware control detuner. This detuner mitigates oversaturation by penalizing large actuator inputs and limiting integrator corrections, at the cost of some flight performance. Together, these measures extend the drone's operational envelope into icing conditions.

The main contributions of this paper are:

1. an experimental methodology for reproducing representative forward-flight loading conditions on a full-UAV test stand in an icing wind tunnel;
2. the integration of information from previous motor–propeller icing experiments, full-UAV test-stand measurements, and data-driven degradation modelling into a simulation-oriented degradation representation;
3. the validation of the degradation representation using full-UAV force, moment, motor-speed, and electrical telemetry data;
4. the incorporation of an ice-mass-based scheduling coordinate as a virtual degradation indicator for characterising the current icing state;
5. the formulation of a controller-design workflow in which clean and degraded models are used for LQR-based, ice-mass-dependent gain scheduling.

2. Methods

2.1 Methodological Overview

The methodological workflow followed in this paper connects experimental icing data, prior degradation modelling, UAV-level simulation, and controller evaluation. First, icing wind-tunnel experiments are used to characterize how propeller ice accretion affects motor speed, motor command, electrical power, and generated force. The experimental data include both single-motor tests for model adaptation and full-UAV test-stand measurements for representative vehicle-level loading conditions. Second, the recorded data are processed and restricted to intervals in which a continuous icing-induced degradation trend is observed. Intervals affected by abrupt ice shedding or active de-icing measures are excluded from the quantitative model adaptation, since the present degradation representation is intended to describe gradual ice accretion rather than stochastic shedding or recovery processes.

Third, a previously identified motor–propeller icing-degradation model is used as a dynamic prior and adapted to the present propulsion configuration. The adaptation is formulated as an output-oriented fitting problem. Starting from the prior model, the simulated motor-speed, electrical-power, force, and degradation-state trajectories are adjusted to match the available target data. The objective is not to identify a fully new physical model or to report all state-space parameters, but to obtain a similarly behaving degradation model that reproduces the relevant input–output trends for controller-oriented simulation.

Fourth, the adapted degradation model is embedded in a six-degree-of-freedom quadrotor simulation model. The simulation focuses on the maximum-payload UAV configuration, since this case represents the most critical condition with respect to remaining propulsion authority. The lighter UAV configuration was not selected for the final comparison because preliminary simulations did not indicate critical actuator limitations.

Fifth, two control strategies are compared. The baseline controller uses a fixed-gain LQR design for the nominal clean configuration. The optimized degradation-aware controller combines degradation-dependent feedback gains with adapted reference velocities in order to reduce the required actuator usage under degraded propulsion conditions.

Finally, the simulation results are evaluated primarily in terms of actuator usage. The main question is whether the UAV can maintain the required flight condition under icing-induced propulsion degradation without reaching the motor-command limit. An additional transient ice-accretion simulation is used to illustrate the degradation mechanism by comparing commanded thrust with the effective thrust generated by the degraded propulsion model.

2.2 Experimental Data Sources and Icing Test-Stand Experiments

The experimental basis of this work consists of three different data sources with distinct roles in the modelling workflow. First, previously acquired motor–propeller icing data provide the prior degradation dynamics used as the starting point for the present model adaptation. Second, a limited set of single-motor icing tests with the present motor–propeller configuration is used to adapt the prior model to the propulsion hardware used in the UAV mock-up. Third, the full-UAV icing test-stand campaign provides UAV-level force, moment, motor-speed, and electrical telemetry data under realistic forward-flight-like loading conditions. The latter data are used to assess the plausibility of the resulting degradation behaviour at vehicle level and to illustrate the asymmetric motor-loading effects that occur in the complete quadrotor configuration.

Table 1 – Experimental data sources and their role in the present work.

Data source	Available information	Role in this paper
Prior motor–propeller icing data	Thrust, motor speed, electrical power, motor command, icing input, terminal ice mass	Prior degradation dynamics from previous work
Target single-motor icing test	Thrust, motor speed, electrical power, motor command, terminal ice mass	Adaptation of the prior model to the present propulsion configuration
Full-UAV test-stand campaign	Forces, moments, motor speeds, motor commands, currents, voltage, icing-cloud activation	Vehicle-level loading context and representative validation of degradation trends
Representative full-UAV run	Time histories of motor current, command, speed, force, and moment response	Illustration of realistic compensation behaviour under icing exposure



Figure 2 – Representative ice accretion on propeller blades observed during the full-UAV icing wind-tunnel campaign. The images illustrate leading-edge ice formation and spanwise ice growth on the rotating propellers. Such accretions modify the effective blade geometry, reduce propulsive efficiency, and increase the electrical power required to maintain the prescribed force and moment conditions.

2.2.1 Test Articles and Instrumentation

The full-UAV experiments were conducted in the climatic and icing wind tunnel at Rail Tec Arsenal (RTA) in Vienna. The test article was a fixed quadrotor mock-up representing a commercial industrial multirotor geometry in the sub-$10\,\mathrm{kg}$ maximum take-off mass class. The mock-up was not intended for autonomous operation and did not include flight-control electronics, navigation sensors, cameras, or payload systems. It was designed for repeatable measurement of UAV-level forces, moments, motor speeds, motor commands, and electrical quantities under icing exposure. Representative propeller ice accretions observed during the campaign are shown in Figure 2.
The UAV mock-up was mounted to the wind-tunnel support through its carbon-fibre bottom plate and connected to an ME-Systeme K6D80 500N/20Nm/MP11 six-component force–torque sensor. A tilting mechanism allowed the rotor plane to be inclined relative to the incoming flow, thereby reproducing a combined axial and cross-flow loading condition representative of forward flight. A photograph of the installed full-UAV mock-up in the icing wind tunnel is shown in Figure 3.

The same measurement and control concept was used for the single-motor and full-UAV test-stand experiments. Data acquisition and real-time control were implemented using Beckhoff EtherCAT I/O modules coupled to a Simulink-based real-time control model. The system generated PWM command signals for the electronic speed controllers and recorded force, moment, motor-speed, voltage, current, electrical-power, and icing-cloud activation signals at $500\,\mathrm{Hz}$. Motor current was measured using LEM HO 50-S Hall-effect transducers. The nominal supply voltage was set to $44.4\,\mathrm{V}$, corresponding to a 12S LiPo battery configuration. The voltage drop along the supply lines was considered in the electrical-power calculation. Even for the highest-load cases, the estimated voltage drop remained below approximately $3\,\%$ of the nominal supply voltage.

2.2.2 Reference Operating Condition and Campaign Envelope

The full-UAV wind-tunnel operating point was derived from outdoor reference flights at a commanded forward velocity of $10\,\mathrm{m\,s^{-1}}$. For this cruise condition, the vehicle exhibited an average forward pitch angle of approximately 10°. The corresponding motor-speed distribution was used to initialize the wind-tunnel test-stand operating point. This links the fixed test-stand experiments to a physically observed flight condition rather than to an arbitrary hover condition.



Figure 3 – Full-UAV quadrotor mock-up mounted on the fixed test stand inside the RTA icing wind tunnel. The setup was used to reproduce representative forward-flight-like loading conditions under controlled icing exposure while measuring UAV-level forces, moments, motor speeds, motor commands, and electrical quantities.

The full-UAV icing campaign comprised 30 test runs. Some operating conditions were repeated to assess repeatability, and additional runs included different de-icing measures. These de-icing configurations are not considered in the present paper and are reserved for future publications. The present work focuses on uncompensated icing-induced propulsion degradation. Consequently, only selected runs and continuous-growth intervals are used for the current model adaptation and validation, while the complete campaign envelope is reported for context.

Table 2 – Unique icing conditions covered during the full-UAV icing campaign. Repeated runs and runs with active de-icing measures are not listed separately.

V_∞ / $\mathrm{m\,s^{-1}}$	T_{amb} / °C	LWC / $\mathrm{g\,m^{-3}}$	MVD / μm
10	-2	0.30	15
10	-2	0.60	20
10	-2	0.30	32
10	-2	0.76	15
10	-5	0.30	15
10	-5	0.53	20
10	-5	0.30	30
10	-5	0.70	15
10	-18	0.30	15
10	-18	0.25	20

2.3 Data Processing and Selection of Continuous-Growth Intervals

The recorded data consist of force and moment measurements, motor-command signals, motor-speed measurements, supply voltage, motor currents, derived electrical power, and the icing-spray activation signal. All signals are synchronized to the common data-acquisition time base and processed at the recorded sampling frequency of $500\,\mathrm{Hz}$. Electrical power is computed from the measured voltage and current signals according to

$$P_{\mathrm{el},i}(t) = U(t)\, I_i(t), \qquad i = 1,\ldots,4, \tag{1}$$

where i denotes the individual motor–propeller unit. If required, the total electrical propulsion power is obtained as

$$P_{\mathrm{el,tot}}(t) = \sum_{i=1}^{4} P_{\mathrm{el},i}(t). \tag{2}$$

The force and moment signals are corrected for the initial sensor offset using a tare interval before the onset of the icing cloud. The resulting time histories are then inspected together with motor current, motor command, motor speed, and the icing-cloud activation signal. Runs with active de-icing measures are not used for the present degradation analysis, since the objective of this work is to model the uncompensated icing-induced propulsion degradation.

The full recorded duration of an icing run is not necessarily used for model adaptation and validation. Instead, the analysis is restricted to intervals in which a continuous degradation trend is observed. This restriction is required because propeller ice accretion does not always evolve monotonically over the complete test duration. In several runs, visual inspection and telemetry indicate abrupt ice-shedding events, where the effective ice mass decreases suddenly, presumably when centrifugal and aerodynamic loads locally exceed ice adhesion. Such events can cause immediate changes in motor current, motor speed, force, or vibration-related quantities and cannot be represented by the monotonic degradation coordinate used in the present model.

Consequently, time intervals affected by pronounced shedding or by de-icing activation are excluded from the quantitative model adaptation and validation. The selected intervals represent phases of gradual ice accretion, during which the increasing electrical demand and the changing motor-speed response can be interpreted as a continuous loss of propulsion effectiveness. This selection is consistent with the intended use of the degradation model as a controller-design model for gradual performance loss.

A more complete description of propeller icing would require an additional stochastic shedding model. Conceptually, such a model could be formulated as an accumulating degradation state with random reset events, similar to Sisyphus random walks or stochastic-resetting processes [12, 13, 14]. Incorporating this reset behaviour is beyond the scope of the present work and is left for future model extensions.

2.4 Prior-Based Degradation Model Adaptation

The degradation model used in this work builds on a previously identified motor–propeller icing model obtained from extensive icing wind-tunnel tests with a larger multicopter propulsion configuration [11]. That prior model describes the coupled evolution of thrust, motor speed, electrical power, and an icing-related degradation state using a discrete-time state-space representation,

$$x_{k+1} = A_0 x_k + B_0 u_k, \tag{3}$$

with the state and input vectors

$$x = \begin{bmatrix} T & n & P & \zeta_{\mathrm{ice}} \end{bmatrix}^{\mathrm{T}}, \qquad u = \begin{bmatrix} u_{\mathrm{PWM}} & q_{\mathrm{ice}} \end{bmatrix}^{\mathrm{T}}. \tag{4}$$

Here, T denotes thrust, n motor speed, P electrical power, and ζ_{ice} a degradation coordinate related to accumulated ice mass. The input u_{PWM} represents the motor command, while q_{ice} represents the icing excitation, which is zero when the icing cloud is inactive.

The prior model was not directly reused for the present UAV configuration, because it was identified for a different motor–propeller system. At the same time, the available data for the present propulsion configuration were too limited for a complete re-identification of all state-space coefficients. Therefore, the prior model was used as the initial model for a constrained trajectory-fitting procedure. The objective was to obtain a similarly behaving degradation model for the present propulsion system, rather than to identify an entirely new model from sparse data.

The adaptation minimizes the deviation between measured and simulated time histories over selected continuous-growth icing intervals. The scalar objective is formulated as a weighted quadratic deviation,

$$J(\theta) = \sum_{k=1}^{N} \left\| W_y \left(y_k - \hat{y}_k(\theta) \right) \right\|_2^2 + J_{\mathrm{ice}}(\theta) + J_{\mathrm{reg}}(\theta), \tag{5}$$

where y_k contains the measured quantities, $\hat{y}_k(\theta)$ denotes the corresponding simulated response of the adapted model, and W_y weights the different output channels. The weighting is used to balance deviations in quantities with different units and magnitudes, such as thrust, motor speed, and electrical power. The structure of the objective is therefore similar to the quadratic performance measure used in LQR design, but here it is applied to model adaptation.

The term J_{ice} accounts for the available terminal ice-mass information, since ice mass was measured only after selected test runs. The regularization term J_{reg} penalizes excessive deviation from the previously identified prior model. In this way, the adaptation remains biased towards the known degradation dynamics while still allowing the model response to match the present motor–propeller configuration.

During adaptation, simple physical constraints are imposed. In particular, the icing-degradation state is allowed to increase only when the icing cloud is active, and no ice growth is generated during cloud-off intervals. Over the selected continuous-growth intervals, the degradation coordinate is constrained to evolve monotonically. Shedding events and active de-icing phases are not included in the fitting data, as described in Section 2.3. Furthermore, the adapted model is constrained to preserve the physically expected signs of the dominant input effects, such as increasing motor speed and electrical power with increasing motor command.

The adapted model is therefore interpreted as a controller-oriented degradation representation. Its purpose is to reproduce the relevant input–output behaviour required for UAV-level simulation and gain-scheduled controller design. The exact numerical state-space parameters are not reported, because the focus of the present work is on the resulting degradation response and its effect on closed-loop performance rather than on the individual fitted coefficients.

2.5 Ice-Mass-Based Scheduling Coordinate

The gain-scheduled controller requires a scalar variable that indicates the current degradation level. In the present work, this variable is based on the accumulated propeller ice mass. The use of such an indirect degradation coordinate is motivated by the fact that propeller icing changes the relation between motor command, rotational speed, generated force, and electrical power. This is consistent with previous performance-based ice-detection approaches, in which icing is inferred from deviations between measured system performance and a reference model [15].

In previous work, ice accretion on a multicopter propulsion system was estimated from propulsion-system telemetry using an LSTM-based sequence-to-single regression model [11]. The estimator maps a time window of motor command, motor speed, voltage, current, and derived electrical power to a scalar ice-mass estimate. In compact form, this can be written as

$$\hat{m}_{\text{ice},k} = f_{\text{LSTM}}\left(\mathbf{s}_{k-N+1}, \ldots, \mathbf{s}_k\right), \tag{6}$$

with the telemetry feature vector

$$\mathbf{s}_k = \begin{bmatrix} u_{\text{PWM},k} & n_k & U_k & I_k & P_{\text{el},k} \end{bmatrix}^{\mathrm{T}}. \tag{7}$$

For a multi-rotor system, the corresponding features can be assembled for each motor–propeller unit. The present paper focuses on the controller-design problem rather than on the ice-mass estimation problem itself. Therefore, the closed-loop simulations use the prescribed ice-mass state as ground truth. This allows the influence of the degradation-dependent controller to be evaluated without introducing additional uncertainty from estimator delay, estimator noise, or false detections.
For gain interpolation, the ice-mass state is converted into a bounded scheduling coordinate,

$$\mu_k = \text{sat}_{[0,1]}\left(\frac{m_{\text{ice},k}}{m_{\text{ice,sched}}}\right), \tag{8}$$

where $m_{\mathrm{ice,sched}}$ denotes the maximum ice-accretion level considered during controller synthesis. The saturation avoids extrapolation of the controller gains beyond the degradation range used for the local LQR designs. Thus, $\mu = 0$ corresponds to the clean propulsion model, whereas $\mu = 1$ corresponds to the maximum degraded operating point considered for gain scheduling.

2.6 Six-Degree-of-Freedom Simulation Model

The adapted degradation model is embedded in a six-degree-of-freedom quadrotor simulation implemented in Simulink. The rigid-body formulation follows the generic multicopter modelling approach used in [9]. The simulation model represents the translational and rotational motion of the UAV, the mapping from rotor forces to generalized forces and moments, and the degradation-dependent propulsion response.

The rigid-body state consists of the inertial position $\mathbf{p}$, inertial velocity $\mathbf{v}$, attitude, and body-fixed angular velocity $\boldsymbol{\omega}$. In compact form, the translational and rotational equations of motion are written as

$$m(t)\dot{\mathbf{v}} = \mathbf{F}_{\mathrm{g}} + \mathbf{R}_{\mathrm{IB}}\mathbf{F}_{\mathrm{B}}, \tag{9}$$

and

$$\mathbf{J}(t)\dot{\boldsymbol{\omega}} = \mathbf{M}_{\mathrm{B}} - \boldsymbol{\omega} \times \mathbf{J}(t)\boldsymbol{\omega}, \tag{10}$$

where $m(t)$ is the vehicle mass, $\mathbf{J}(t)$ the inertia matrix, $\mathbf{F}_{\mathrm{g}}$ the gravitational force, $\mathbf{R}_{\mathrm{IB}}$ the rotation matrix from body-fixed to inertial coordinates, $\mathbf{F}_{\mathrm{B}}$ the force vector expressed in the body-fixed frame, and $\mathbf{M}_{\mathrm{B}}$ the corresponding body-fixed moment vector. The clean mass and inertia properties of the UAV mock-up are obtained from a CAD-based estimate.

The four rotor forces are mapped to the generalized force and moment vector by the quadrotor allocation model,

$$\mathbf{w} = \begin{bmatrix} F_z & M_x & M_y & M_z \end{bmatrix}^{\mathrm{T}} = \mathbf{B}_{\mathrm{alloc}}\mathbf{f}_{\mathrm{rotor}}, \tag{11}$$

where $\mathbf{f}_{\mathrm{rotor}}$ contains the individual rotor thrust contributions. Under icing conditions, the rotor thrust and power response are not assumed to remain nominal. Instead, the clean propulsion representation is replaced by the adapted degradation model described in Section 2.4. The model therefore changes the effective relation between motor command, motor speed, generated thrust, and electrical power as the icing state evolves.

In the icing cases, the prescribed ice state drives the degradation model during an initial hover phase and throughout the subsequent manoeuvre. The accumulated body-ice mass does not feed back into the aerodynamic model. Thus, changes in airframe shape, drag, and local aerodynamic moments due to ice accretion are not considered. This simplification isolates the effect of propulsion degradation on the closed-loop response.

The resulting simulation model provides a controlled environment for evaluating how icing-induced changes in propulsion effectiveness influence trajectory tracking, attitude response, actuator usage, and electrical power demand. It is therefore used as the basis for the baseline and gain-scheduled controller comparison described in the following sections.

2.7 Baseline and Optimized Degradation-Aware Control

The controller comparison considers two control strategies. The first strategy is a fixed-gain baseline controller. It uses one LQR feedback gain designed for the nominal clean UAV model and applies the same reference trajectory and reference velocities in all simulated cases. This controller therefore represents a conventional design that does not explicitly account for icing-induced propulsion degradation.

The second strategy is an optimized degradation-aware controller. In this case, the controller adaptation is not limited to the feedback gain. In addition to using degradation-dependent LQR gains, the reference velocities along the manoeuvre are adjusted to reduce the required actuator usage under degraded propulsion conditions. The optimized controller therefore represents a combined gain- and reference-adaptation strategy. Its objective is not only to track the geometric reference path, but to keep the commanded motor inputs within the available actuator authority when the propulsion system

is degraded by ice accretion.

For compact notation, the local LQR design is formulated in deviation coordinates. In the following, $\mathbf{x}$ and $\mathbf{u}$ denote deviations from the corresponding trim or reference condition, i.e., $\mathbf{x} = \mathbf{x}_{\text{abs}} - \mathbf{x}_{\text{ref}}$ and $\mathbf{u} = \mathbf{u}_{\text{abs}} - \mathbf{u}_{\text{trim}}$. The absolute motor commands applied in simulation are obtained by adding the trim input corresponding to the current reference condition.
For each considered operating condition, the nonlinear simulation model is linearized around a trimmed operating point. Each local operating point is defined by the UAV mass configuration and the degradation level. The corresponding local linear model is written as

$$\dot{\mathbf{x}} = \mathbf{A}_j \mathbf{x} + \mathbf{B}_j \mathbf{u}, \tag{12}$$

where the index j denotes the selected local operating point. The matrices $\mathbf{A}_j$ and $\mathbf{B}_j$ are obtained from the same linearization point and therefore represent one consistent local model.
For each local model, a continuous-time LQR gain is computed by minimizing the standard quadratic cost function

$$J = \int_0^\infty \left(\mathbf{x}^{\mathrm{T}} \mathbf{Q} \mathbf{x} + \mathbf{u}^{\mathrm{T}} \mathbf{R} \mathbf{u} \right) \mathrm{d}t. \tag{13}$$

The formulation follows the standard continuous-time LQR framework based on the algebraic Riccati equation; complete derivations are given by Anderson and Moore [16] and Lewis et al. [17]. The resulting local feedback law is

$$\mathbf{u} = -\mathbf{K}_j \mathbf{x}. \tag{14}$$

The matrices $\mathbf{Q}$ and $\mathbf{R}$ define the relative weighting of state deviations and control effort. The same weighting philosophy is retained for all local LQR designs, so that differences between the resulting feedback gains are caused by changes in the operating condition rather than by manual retuning of the cost function.
For the degradation-aware controller, the applied gain is selected according to the icing-degradation coordinate μ. In the simplest case with one clean and one degraded design point, the scheduled gain is obtained by linear interpolation,

$$\mathbf{K}(\mu) = (1-\mu)\,\mathbf{K}_0 + \mu \mathbf{K}_1, \qquad 0 \le \mu \le 1, \tag{15}$$

where $\mathbf{K}_0$ denotes the gain for the clean propulsion model and $\mathbf{K}_1$ denotes the gain for the degraded propulsion model. The scheduled feedback law is therefore

$$\mathbf{u} = -\mathbf{K}(\mu)\mathbf{x}. \tag{16}$$

For manoeuvre tracking, the controller is applied in a multi-setpoint form. The reference path is represented by a sequence of local reference states. In the baseline case, the nominal reference velocities are retained. In the optimized case, the reference velocities are adjusted together with the degradation-aware feedback gains in order to reduce peak actuator usage under degraded propulsion conditions.
The comparison in this work therefore evaluates whether the optimized degradation-aware controller preserves sufficient actuator authority under icing-induced performance loss. It does not assess controllability in the strict linear-systems sense, such as by evaluating the rank of the controllability matrix. Instead, the closed-loop simulations are used to determine whether the required motor commands remain below the available actuator limits.

2.8 Simulation Scenarios and Evaluation Metrics

The closed-loop simulation study focuses on the maximum-payload UAV configuration. This case represents the most critical operating condition with respect to available propulsion margin, since the vehicle mass is highest and less actuator reserve remains available. Preliminary simulations with lower take-off mass did not indicate critical actuator limitations and are therefore not included in the final comparison.

The reference manoeuvre is defined as an axis-aligned cube-edge trajectory. The UAV follows consecutive $10\,\mathrm{m}$ translation segments in the principal directions: forward, rightward, upward, leftward, backward, and downward. This trajectory combines the main translational flight directions in one compact scenario and requires the controller to redistribute thrust and moments during changes in flight direction.
Three main simulation cases are considered. The first case represents the clean UAV with the fixed-gain baseline controller and serves as the nominal reference. The second case uses the same baseline controller, but assumes pre-accreted ice, such that the propulsion model is degraded from the beginning of the manoeuvre. The third case uses the same pre-accreted icing condition, but applies the optimized degradation-aware controller described in Section 2.7. In addition, one transient ice-accretion simulation is included to illustrate the degradation process itself. In this case, the ice state increases during the simulation and the controller must increase the commanded propulsion effort to compensate for the reduced effective thrust.

Table 3 – Simulation cases considered for the maximum-payload UAV configuration.

Case	Icing state	Controller strategy
Clean baseline	No ice	Fixed-gain baseline controller
Iced baseline	Pre-accreted ice	Fixed-gain baseline controller
Iced optimized	Pre-accreted ice	Optimized degradation-aware controller
Accretion transient	Ice accretes during simulation	Selected controller strategy

The evaluation focuses on actuator usage rather than on trajectory-tracking accuracy. The objective is to assess whether the UAV can maintain the required flight condition under degraded propulsion performance without reaching the available motor-command limit. The primary time-history metric is the maximum normalized motor command over all four rotors,

$$u_{\max}(t) = \max_{i=1,\dots,4} u_i(t), \tag{17}$$

where $u_i(t)$ denotes the normalized command of the i-th motor. In the present work, motor commands are expressed in percent. Therefore, $100\,\%$ represents the available actuator command limit, and values approaching this limit indicate operation close to saturation.
For compact comparison, the peak actuator usage is evaluated as

$$u_{\max,\mathrm{peak}} = \max_{t\in[t_0,t_f]} u_{\max}(t). \tag{18}$$

This scalar value provides a direct measure of the highest propulsion demand occurring during the manoeuvre.
For the transient ice-accretion case, commanded and effective thrust are compared. The commanded thrust represents the thrust requested by the controller, whereas the effective thrust represents the thrust generated by the degraded propulsion model and available for the UAV dynamics. The difference between both quantities illustrates how icing-induced propulsion degradation reduces the effective force available to control the vehicle and why increasing actuator demand is required to maintain the flight condition.

The simulation results are therefore interpreted in terms of actuator usage and remaining propulsion authority. The analysis does not assess controllability in the strict linear-systems sense, but evaluates whether the closed-loop system can maintain the required flight condition without reaching the motor-command limit.

3. Results

The results are presented in four steps. First, the adaptation of the previously identified rotor-level degradation model to the present propulsion configuration is evaluated. Second, the ice-mass accumulation coefficient used in the subsequent simulations is reported. Third, the closed-loop tracking

performance of the baseline and gain-scheduled controllers is compared for the simulation cases defined in Section 2.8. Finally, actuator usage and scalar performance metrics are used to assess the remaining control margin under icing-induced propulsion degradation.

3.1 Adaptation of the Prior Degradation Model

The previously identified propulsion-degradation model from [11] was adapted to the propulsion configuration of the present UAV mock-up. Since only three suitable icing runs were available for the motor–propeller combination used in this work, the model was not re-identified from scratch. Instead, the prior state-space model was used as the initial estimate and adjusted to reproduce the measured response of the present configuration during selected continuous-growth icing intervals.

Figure 4 compares the measured and reconstructed trajectories for one representative case used to evaluate the adapted model. The adapted model reproduces the dominant degradation trends observed in the experiment, including the gradual changes in thrust, motor speed, and electrical power. The terminal ice mass is also represented by the reconstructed degradation state. Local transient behaviour is not matched exactly, because the adaptation uses one global objective that balances deviations across all considered signals.

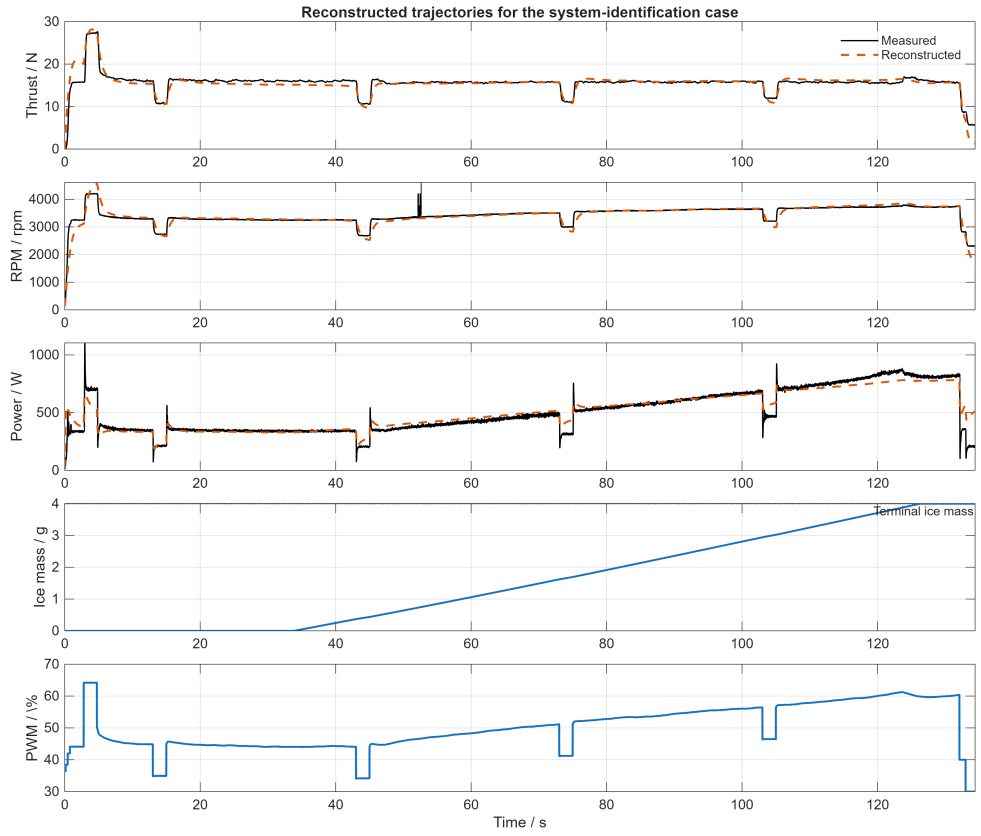


Figure 4 – Measured and reconstructed trajectories for a representative icing run used to evaluate the adaptation of the prior degradation model to the present propulsion configuration. The figure shows thrust, motor speed, electrical power, ice mass, and commanded PWM. The adapted model captures the dominant degradation trend, while local transient behaviour is not fully reproduced because the optimization balances all considered signals within one global objective.

The adapted model is therefore interpreted as a transferred degradation model with similar dynamic behaviour for the present propulsion configuration, rather than as an independently identified model based on an extensive motor dataset. For this reason, the exact numerical state-space parameters are not reported in the main text. The model is used in the following sections as a degradation coordinate for gain scheduling and closed-loop simulation.

3.2 Ice-Mass Accumulation Coefficient

The ice-mass accumulation coefficient used in the subsequent simulations was estimated from the available propeller icing runs. The accumulation model assumes that the ice-mass flow rate is proportional to the liquid water content and to the propeller angular speed,

$$\dot{m}_{\mathrm{ice}}(t) = c_{\mathrm{ice},\omega}\, \chi_{\mathrm{spray}}(t)\, \mathrm{LWC}(t)\, \omega(t), \tag{19}$$

where $\chi_{\mathrm{spray}}(t) \in \{0,1\}$ denotes the effective spray-cloud activation signal, including the applied activation and deactivation lag, $\mathrm{LWC}(t)$ is the liquid water content, and $\omega(t)$ is the propeller angular speed. Integration over one icing run gives

$$\Delta m_{\mathrm{ice}} = c_{\mathrm{ice},\omega} \int_{t_0}^{t_1} \chi_{\mathrm{spray}}(t)\, \mathrm{LWC}(t)\, \omega(t)\, \mathrm{d}t. \tag{20}$$

The coefficient for each run r was therefore obtained from the measured terminal ice mass according to

$$c_{\mathrm{ice},\omega}^{(r)} = \frac{m_{\mathrm{ice,final}}^{(r)} - m_{\mathrm{ice},0}^{(r)}}{\displaystyle\int_{t_0^{(r)}}^{t_1^{(r)}} \chi_{\mathrm{spray}}^{(r)}(t)\, \mathrm{LWC}^{(r)}(t)\, \omega^{(r)}(t)\, \mathrm{d}t}. \tag{21}$$

With m_{ice} expressed in grams, LWC in $\mathrm{g\,m^{-3}}$, and ω in $\mathrm{rad\,s^{-1}}$, the coefficient has the formal unit $\mathrm{m^3\,rad^{-1}}$.

Only three suitable icing runs were available, due to the limited availability of icing-wind-tunnel test time and the associated experimental infrastructure. The representative coefficient was obtained as the arithmetic mean,

$$c_{\mathrm{ice},\omega} = \frac{1}{N_r} \sum_{r=1}^{N_r} c_{\mathrm{ice},\omega}^{(r)}, \qquad N_r = 3. \tag{22}$$

The resulting value was

$$c_{\mathrm{ice},\omega} = 1.61 \times 10^{-4}\,\mathrm{m^3\,rad^{-1}}. \tag{23}$$

This value is used for the continuous-time simulations presented in the following sections. It is close to the value obtained from the most carefully curated and documented individual run, $c_{\mathrm{ice},\omega} = 1.64 \times 10^{-4}\,\mathrm{m^3\,rad^{-1}}$, which supports its use as a representative coefficient for the present data set. The coefficient should nevertheless be interpreted as an empirical parameter for the present propulsion configuration and test conditions, rather than as a general ice-accretion law.

3.3 Representative Full-UAV Icing Behaviour

Figure 1 shows a representative full-UAV icing test run from the wind-tunnel campaign. The run is not used as the primary identification data set, but illustrates how icing-induced propulsion degradation appears at vehicle level under forward-flight-like loading conditions. During the icing-cloud interval, motor current, motor command, and motor speed increase while the test-stand controller maintains the prescribed force and moment conditions. This indicates that the propulsion system compensates for the degraded propeller state by increasing actuator effort and electrical power demand.

The run also shows a difference between the front and rear propellers. This is consistent with the thrust redistribution required to maintain the pitching moment in forward-flight-like conditions. The stronger increase observed at the rear propellers can be interpreted as an indication of higher local loading and larger degradation effects. A possible explanation is that the higher rear propeller speed promotes stronger local ice accretion, which further reduces propulsive efficiency and increases the required electrical power.

3.4 Transient Ice-Accretion Response

The transient ice-accretion simulation illustrates how the degradation develops during continued icing exposure. In this case, the ice state increases during the simulation and the propulsion model gradually loses effectiveness. The controller reacts by increasing the commanded motor output in order to maintain the required force and moment response.

Figure 5 shows the commanded motor signal together with the increasing ice state. The result demonstrates that the required actuator effort rises as the degradation state develops. This behaviour is consistent with the representative full-UAV wind-tunnel run shown in Figure 1, where motor current, motor command, and motor speed increase during the active icing-cloud interval.

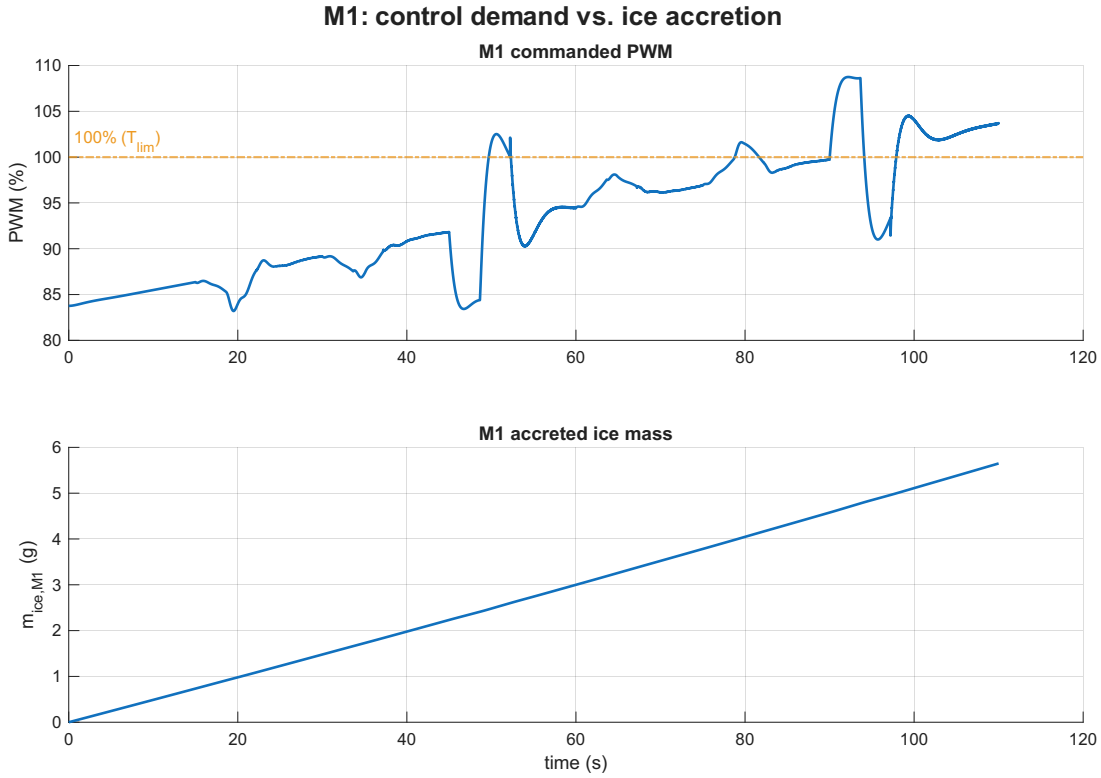


Figure 5 – Transient ice-accretion simulation showing the increase of the commanded motor signal as the ice state develops. The rising command level reflects the additional actuator effort required to compensate for icing-induced propulsion degradation.

The degradation mechanism is further illustrated by comparing commanded and effective thrust. The commanded thrust represents the force requested by the controller, whereas the effective thrust represents the thrust generated by the degraded propulsion model and available for the UAV dynamics. As ice accretes, the same commanded propulsion effort produces less effective thrust. The controller must therefore increase the commanded output to maintain the flight condition.
These results show that icing-induced degradation appears to the flight controller as a reduction in effective actuator authority. Even before actuator saturation is reached, the controller has to request higher motor commands and, consequently, higher electrical power to maintain the same flight condition.

3.5 Actuator Usage during an Evasive Return Manoeuvre

The second simulation scenario considers a UAV that has already accumulated ice before the manoeuvre starts. This represents a post-detection situation in which the UAV is assumed to have recognized that it is operating in icing conditions and then performs an evasive return manoeuvre to leave the affected region. The scenario is not intended to define an operational procedure, but to evaluate whether sufficient actuator authority remains available after propulsion degradation has already developed.

The comparison is performed for the maximum-payload UAV configuration, since this represents the most critical case with respect to propulsion margin. Three cases are considered: the clean UAV with the baseline controller, the iced UAV with the same baseline controller, and the iced UAV with the optimized degradation-aware controller. The optimized controller combines degradation-dependent feedback gains with adjusted reference velocities in order to reduce peak actuator usage

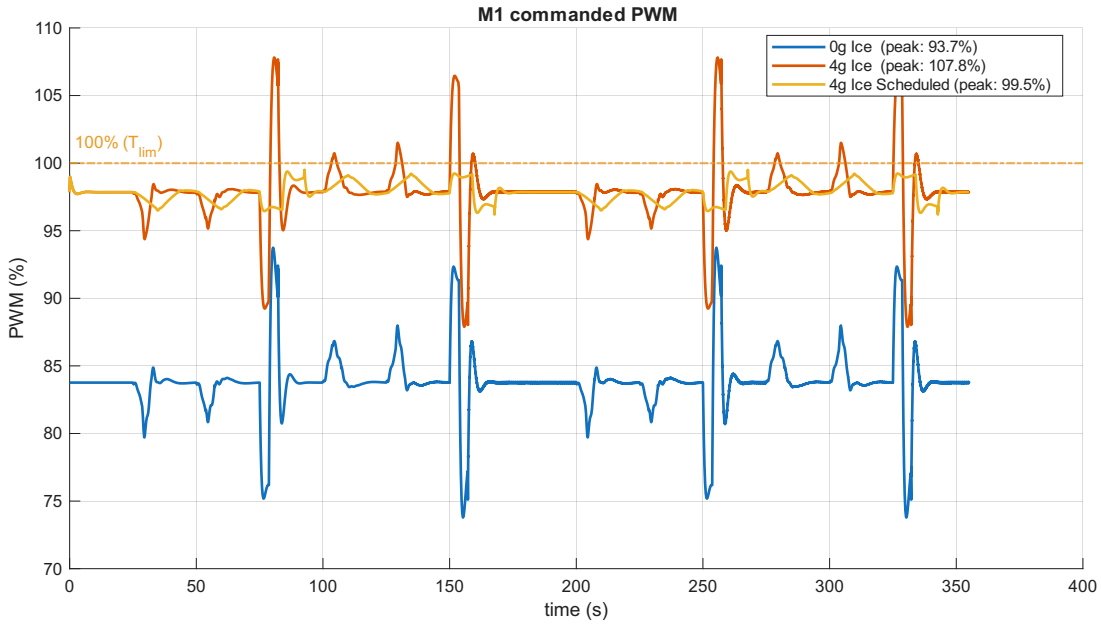


Figure 6 – Commanded and effective propulsion response during the transient ice-accretion simulation. The difference between the controller command and the effective thrust-producing response illustrates the loss of propulsion effectiveness caused by ice accretion.

under degraded propulsion conditions.
The actuator usage is represented by the maximum commanded motor signal over all four rotors,

$$u_{\max}(t) = \max_{i=1,\dots,4} u_i(t), \tag{24}$$

where $u_i(t)$ denotes the commanded motor signal of rotor i, expressed in percent of the available command range. Since $100\,\%$ corresponds to the actuator command limit, values approaching this limit indicate operation close to saturation.
Figure 7 compares the maximum motor command during the evasive return manoeuvre. The clean baseline case provides the nominal reference. In the iced baseline case, the controller must compensate for the reduced propulsion effectiveness using the same nominal control strategy, which leads to increased actuator usage. The optimized degradation-aware controller reduces the required command level by adapting the control strategy to the degraded propulsion state.
The results indicate that the main limitation under pre-accreted icing is the remaining actuator authority rather than nominal trajectory-tracking accuracy. Since the LQR design penalizes control effort but does not impose hard actuator constraints, operation close to the command limit is not excluded by the controller design itself. The maximum motor command therefore provides a practical feasibility indicator for the simulated evasive manoeuvre.

The increased actuator usage also implies increased electrical power demand. Although the remaining mission duration is not explicitly modelled in this work, the representative full-UAV test-stand data in Figure 1 show that maintaining force and moment conditions under icing can require a pronounced increase in electrical demand. Thus, even if the UAV remains controlled in simulation, the reduced remaining energy reserve and the additional electrical or thermal loading of motors, ESCs, connectors, and supply lines may become limiting factors. These effects are not investigated here, since the test stand was operated with sufficient power reserves and the electrical components were not tested to failure.

4. Discussion

The results show that a previously identified propulsion-degradation model can be transferred to the present UAV configuration in a controller-oriented manner. Although only limited data were available for the motor–propeller system used in the full-UAV mock-up, the adapted model reproduces

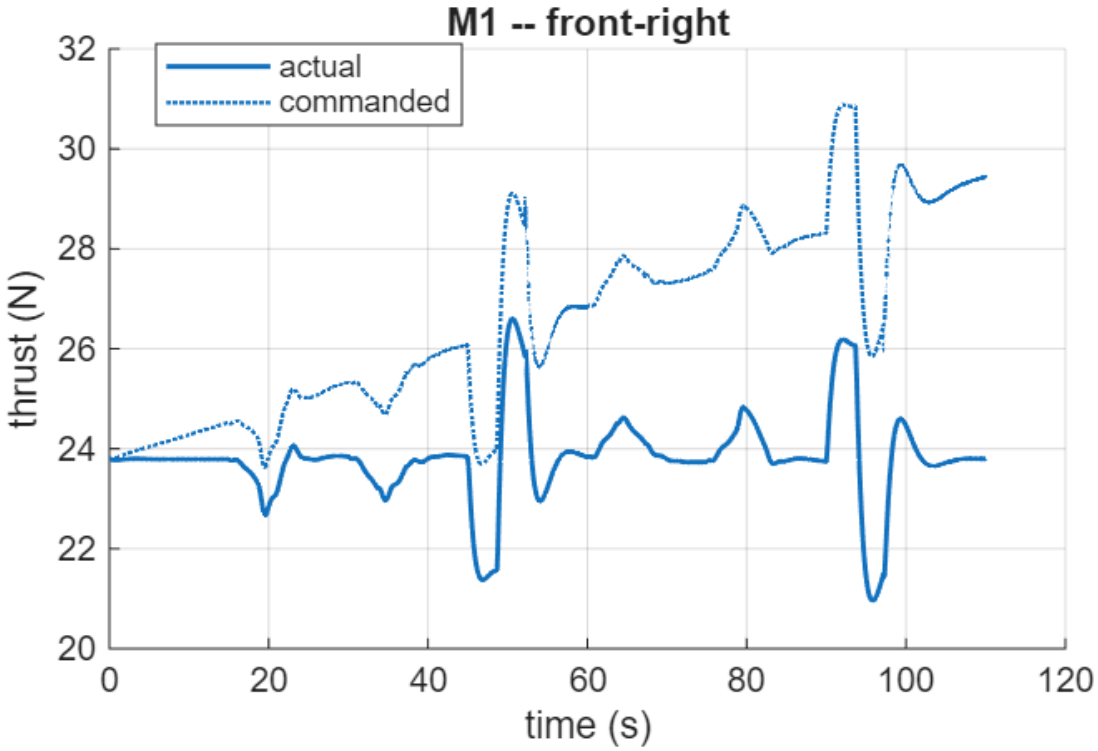


Figure 7 – Maximum motor command during the evasive return manoeuvre for the maximum-payload UAV configuration. The comparison shows the clean baseline case, the pre-accreted icing case with the baseline controller, and the pre-accreted icing case with the optimized degradation-aware controller. Motor command is expressed in percent of the available command range, with $100\,\%$ corresponding to the actuator command limit.

the dominant degradation trend observed during the selected continuous-growth icing interval. The model should therefore be interpreted as a pragmatic model-transfer step rather than as a complete re-identification of the present propulsion system.

The transient ice-accretion simulation illustrates the main effect of propeller icing from the controller perspective. As ice accumulates, the same commanded propulsion effort produces less effective thrust. The controller must therefore increase the commanded motor output to maintain the required force and moment response. This behaviour is consistent with the representative full-UAV wind-tunnel run, where motor current, motor command, and motor speed increase during the active icing-cloud interval while the prescribed loading condition is maintained.

The pre-accreted icing simulations show that this reduction in propulsion effectiveness becomes critical for the maximum-payload UAV configuration. The baseline controller can maintain the considered manoeuvre in simulation, but it requires substantially higher motor commands and operates closer to the actuator command limit. The optimized degradation-aware controller reduces the required actuator usage by combining adapted feedback gains with modified reference velocities. The main benefit is therefore interpreted as an increase in remaining propulsion authority, rather than primarily as an improvement in nominal tracking accuracy.

This analysis does not assess controllability in the strict linear-systems sense. No controllability-rank condition is evaluated, and no formal global stability proof is provided. Instead, the simulations evaluate whether the required motor commands remain below the available actuator command limit during the considered evasive manoeuvre. This is a practical feasibility criterion for the present application, since actuator saturation would directly limit the ability of the UAV to maintain the required force and moment response.

The observed increase in electrical demand is consistent with RPAS icing tests reported by Orchard, where maintaining thrust under icing required increased torque and power, and where full-RPAS hover tests showed pronounced motor-power increase before loss of sustained hover capability [6, 7]. Even if the UAV remains controlled in simulation, the increased electrical power demand reduces the remaining mission duration and may increase thermal and electrical loading of motors, ESCs, connectors, and supply wiring. These effects are not explicitly investigated here, since the test stand had sufficient power reserves, the electrical components were not tested to failure, and the simulation model does not include a battery model.

Several limitations remain. Ice accretion on the UAV body is represented only as an additional mass contribution; changes in aerodynamic shape, drag, and moment characteristics are not modelled. The prescribed ice-mass state is used directly as scheduling information, thereby isolating the controller-design problem from the separate ice-estimation problem. In addition, abrupt ice-shedding events are excluded from the quantitative model adaptation. Capturing such behaviour would require a stochastic reset model, for example a Sisyphus-random-walk-like process or an integrator with random reset, and is left for future work.

Overall, the study demonstrates a path from experimentally observed icing-induced propulsion degradation to controller-oriented simulation and degradation-aware control adaptation. Future work should extend the experimental database for the present configuration, include aerodynamic and electrical energy-storage effects, and validate the proposed control concept in hardware-in-the-loop or free-flight experiments.

Acknowledgements

The work was conducted within the projects “**IceDrone**” and “**IFIRE**”. The project IceDrone has received funding from the Austrian research funding program “Take Off” under grant agreement No. FO999902894. The project IFIRE has received funding from the Austrian research funding program “Take Off” under grant agreement No. FO999914003. “Take Off” is a Research, Technology and Innovation Funding Program of the Republic of Austria, Ministry of Climate Action. The Austrian Research Promotion Agency (FFG) has been authorized for the program management.

Contact Author Email Address

arno.fallast@fh-joanneum.at

Copyright Statement

The authors confirm that they, and/or their company or organization, hold copyright on all of the original material included in this paper. The authors also confirm that they have obtained permission, from the copyright holder of any third party material included in this paper, to publish it as part of their paper. The authors confirm that they give permission, or have obtained permission from the copyright holder of this paper, for the publication and distribution of this paper as part of the ICAS proceedings or as individual off-prints from the proceedings.

References

[1] Mozhou Gao, Chris H. Hugenholtz, Thomas A. Fox, Maja Kucharczyk, Thomas E. Barchyn, and Paul R. Nesbit. Weather constraints on global drone flyability. *Scientific Reports*, 11(1):12092, Jun 2021.

[2] Unisphere GmbH. Global Icing Report for Air Taxi Services: Examining 30 UAM Cities. White paper, 2023.

[3] European Aviation Safety Agency. Certification Specifications and Acceptable Means of Compliance for Large Aeroplanes CS-25 Amendment 19. URL: https://www.easa.europa.eu/system/files/dfu/CS-25 Cited: 15 June 2017.

[4] Ricardo Solís, Lizeth Torres, and Pablo Pérez. Review of methods for diagnosing faults in the stators of bldc motors. *Processes*, 11(1), 2023.

[5] Jinquan Xuan, Xiaohong Wang, Dawei Lu, and Lizhi Wang. Research on the safety assessment of the brushless dc motor based on the gray model. *Advances in Mechanical Engineering*, 9(3):1687814017695438, 2017.

[6] David Orchard. Development of an icing test facility for rotors and propellers of remotely piloted aircraft systems (rpas). In *SAE International Conference on Icing of Aircraft, Engines, and Structures*, 2023.

[7] David Orchard. Development of a test rig for the assessment of remotely piloted aircraft systems (rpas) in icing. In *SAE International Conference on Icing of Aircraft, Engines, and Structures*, 2023.

[8] David Kozomara, Jakob R. Amon, Reinhard Puffing, Richard Moser, Wolfgang Breitfuss, Thomas Neubauer, Simon Schweighart, Ingeborg Bednar, and Stephan Thein. *Experimental Investigation of a Quadcopter UAS With a Fluid-Based De-Icing System in Appendix C Icing Conditions*.

[9] B. Messnarz, A. Fallast, and M. Mocher. Modellierung und simulation eines vollständig aktuierten multirotor-uavs. *Deutscher Luft- und Raumfahrt-Kongress DLRK2016*, 2016.

[10] Arno Fallast, Marcell Mo, and Bernd Messnarz. Efficiency measurements of coaxial multi-rotor propulsion systems. In *Proceedings of the Deutscher Luft- und Raumfahrtkongress (DLRK) 2016*, Braunschweig, Germany, September 2016.

[11] Arno Fallast and Arian Ghoddousi. System identification of a multicopter powertrain with degradation for simulation-based training of a fault detection neural network. In *AIAA AVIATION FORUM AND ASCEND 2024*.

[12] Miquel Montero and Javier Villarroel. Directed random walk with random restarts: The Sisyphus random walk. *Physical Review E*, 94(3):032132, 2016.

[13] Martin R. Evans, Satya N. Majumdar, and Grégory Schehr. Stochastic resetting and applications. *Journal of Physics A: Mathematical and Theoretical*, 53(19):193001, 2020.

[14] Marcin Magdziarz and Kacper Taźbierski. Stochastic representation of processes with resetting. *Physical Review E*, 106(1):014147, 2022.

[15] Christoph Deiler and Falk Sachs. Design and testing of an indirect ice detection methodology. In *SAE International Conference on Icing of Aircraft, Engines, and Structures*, 2023.

[16] Brian D. O. Anderson and John B. Moore. *Optimal Control: Linear Quadratic Methods*. Dover Publications, Mineola, NY, 2007.

[17] Frank L. Lewis, Draguna L. Vrabie, and Vassilis L. Syrmos. *Optimal Control*. John Wiley & Sons, Hoboken, NJ, 3 edition, 2012.